Computational approaches revealing potential anti-HMPV therapeutic candidates

Quan Ke Thai[1]*, Phuoc Huynh[2] and Hien Pham Thi Thanh[1]
1. Faculty of Natural Science Education, Saigon University, 273 An Duong Vuong, Cho Quan Ward, Ho Chi Minh City, 700000, VIETNAM
2. Graduate University of Science and Technology, Vietnam Academy of Science and Technology, VIETNAM
*tkquan@sgu.edu.vn

Abstract
Human metapneumovirus (HMPV) has emerged as a significant respiratory pathogen with substantial clinical and public health implications. Despite its widespread circulation in many countries, no specific antiviral drugs or vaccines have been approved for HMPV treatment. Therefore, identifying repurposed drugs with potential efficacy against HMPV represents a rational strategy to accelerate drug development. In this study, we employed 2,118 molecules of the e-Drug3D library comprising of FDA-approved drugs to the HMPV CR-VI protein structure (MTase). This protein plays a crucial role in viral RNA synthesis by catalyzing the methylation of the RNA cap at the 2'O and N7 positions. Our virtual screening results identified the antiviral agents PIBRENTASVIR, ELBASVIR, RITONAVIR and REMDESIVIR as high-affinity binders to MTase through interactions with its catalytic sites, ^{SAM}P and ^{SUB}P. Molecular dynamics simulations demonstrated that PIBRENTASVIR, RITONAVIR and REMDESIVIR form stable interactions within the MTase binding pocket.

Furthermore, binding free energy analysis revealed strong binding affinities and competitive interactions with the MTase active site, particularly with GTP. This study provides the evidence of these molecules as potential MTase inhibitors. Our findings establish an initial framework for further screening and clinical evaluation, contributing to the development of effective anti-HMPV therapeutics.

Keywords: Antiviral drugs, Dynamic simulation, Human metapneumovirus (HMPV), MTase, Molecular docking.

Introduction

Human metapneumovirus (HMPV) was first identified in 2001 by a research group in the Netherlands[34]. Since then, it has been recognized as a causative agent of acute respiratory tract infections (ARTIs)[34], which contribute to high morbidity and mortality rates in humans. ARTIs are considered one of the most critical threats to global public health[12]. HMPV has increasingly gained recognition as a significant respiratory pathogen with substantial clinical and public health implications[5]. The circulation of HMPV has been reported in multiple countries and is regarded as a leading cause of ARTIs worldwide, largely due to limited preventive and control measures[6,7].

Despite its global prevalence and the considerable healthcare burden it imposes on local populations, no effective vaccines or antiviral drugs have been officially approved for the treatment or prevention of HMPV infection[17]. Therefore, the identification of potential therapeutic molecules against HMPV is a crucial objective in efforts to mitigate viral transmission and associated health risks.

HMPV is an enveloped virus with a negative-sense single-stranded RNA genome, classified under the family *Pneumovirinae* within the order *Mononegavirales*[3]. Its genome is approximately 13,000 nucleotides in length and encodes eight genes, which translate into nine proteins: nucleoprotein (N), phosphoprotein (P), matrix protein (M), fusion protein (F), matrix-2 proteins (M2-1 and M2-2), small hydrophobic protein (SH), glycoprotein (G) and large (L) polymerase protein[28,33].

Among these, the L protein plays a crucial role in viral replication by performing both RNA transcription and replication[21]. Specifically, the CR-VI (MTase) domain of the HMPV L protein has been identified as a methyltransferase, with its activity dependent on the catalytic sites: S-adenosylmethionine-binding site (^{SAM}P) and the ^{SAM}P-adjoining site holding the nucleotides undergoing methylation (^{SUB}P)[21]. This domain is involved in the capping process by catalyzing the synthesis of fully methylated RNA cap structures[21,25]. Furthermore, these catalytic pockets are conserved across HMPV and other viruses within the *Mononegavirales* order[21], making MTase an attractive target for broad-spectrum antiviral drugs and novel drug design efforts.

Drug repurposing, an approach that identifies new therapeutic uses for existing drugs, has emerged as a promising strategy to accelerate the availability of treatments[15]. In this study, we utilized FDA-approved antiviral drugs from the e-Drug3D database[24] targeting the catalytic site of MTase. Using the broad-spectrum antiviral is REMDESIVIR (GS-5734) which has been employed against RNA virus families, including positive-sense *Coronaviridae* and *Flaviviridae* as well as negative-sense *Filoviridae* and *Pneumoviridae* to predict the ability of this drug against HMPV[36]. The repurposing of these compounds for HMPV leverages their known mechanisms of action and established safety profiles, expediting their potential clinical application.

**** Author for Correspondence***

Material and Methods

Protein and ligands preparation: The MTase structure was obtained from the Protein Data Bank (PDB ID: 4UCZ)[21]. The MTase was prepared using Autodock tools[19] where hydrogen atoms were added to the protein and its charges were balanced using the Gasteiger algorithm. The protein model was then converted into a suitable format for virtual screening. The drug library was retrieved from the e-Drug3D database[24]. Molecular structures were energy-minimized until reaching an equilibrium state using the MMFF94 force field in OpenBabel software[20]. A total of 2,118 molecular structures from e-Drug3D were utilized for screening.

Molecular docking: The active sites of MTase including the ^{SAM}P, the novel pocket (^{NS}P) and ^{SUB}P[21], were designated as docking targets. Docking simulations were performed using AutoDock GPU[26]. The docking grid was positioned at coordinates x = 25.484, y = -11.960 and z = -50.049, with a box size of 70 × 70 × 70 and a spacing of 0.375 Å. Each ligand was subjected to 100 docking simulations (n_run = 100) and the conformation with the lowest predicted free energy was chosen for each molecule. The compounds with the strongest binding affinity to MTase were selected for further evaluation. Protein-ligand interactions were assessed using the Protein-Ligand Interaction Profiler (PLIP) server[2].

Molecular dynamics simulation: Molecular dynamics (MD) simulations were performed using GROMACS version 2023.5[1]. The MD system was set up using the CHARMM-GUI server[14] with default parameters. Specifically, the MD was calculated using the ff19sb force field, solvated with the four-site OPC model for high precision[29] with a NaCl concentration of 0.15 M. Energy minimization (EM) was applied to relax the systems until they reached a stable energy state. Subsequently, the system was accelerated to achieve temperature equilibrium at 300 K and pressure at 1 atm over 125 ps, using the V-rescale thermostat and C-rescale barostat. The production phase was executed for 100 ns with a time step of 2 fs. Long-range electrostatic interactions were calculated using the Particle Mesh Ewald (PME) method with a Coulomb cutoff of 0.9 nm and short-range van der Waals interactions were truncated at 0.9 nm.

The LINCS algorithm was employed to maintain holonomic constraints and trajectory sampling occurred every 10 ps. Post-simulation analysis was performed using GROMACS utilities, with principal component analysis (PCA) conducted to assess ligand movement convergence within each system using MDTraj software[18].

Binding free energy calculation: The free energy of ligand binding to the MTase was estimated using the gmx_MMPBSA software[31]. The MM/GBSA algorithm was employed with default parameters and the MM/GBSA equation was computed as follows:

$$\Delta G_{MM/GBSA} = \Delta G_{Complex} - \Delta G_{Protein} - \Delta G_{ligand}$$

Each component of the total free energy was calculated using the formula:

$$\Delta G = \Delta G_{vdW} + \Delta G_{ele} + \Delta G_{pol} + \Delta G_{npol}$$

where ΔG_{ele} and ΔG_{vdW} represent electrostatic and Van der Waals interactions energies the protein and ligand respectively while ΔG_{pol} and ΔG_{npol} account for the polar and non-polar solvation free energy contributions. Free energy decomposition per residue was performed to identify the key amino acids involved in interactions between the protein and ligand.

Results and Discussion

Molecular docking: Based on the free energy of binding data, we selected the three antiviral compounds with the highest binding affinity to MTase, along with the broad-spectrum antiviral REMDESIVIR, for further analysis. The three selected antiviral compounds were PIBRENTASVIR (-19.2 kcal/mol), ELBASVIR (-16.42 kcal/mol) and RITONAVIR (-15.61 kcal/mol). REMDESIVIR also demonstrated binding to MTase with an affinity of -13.20 kcal/mol. Binding state analysis revealed that these molecules were well-positioned within distinct binding pockets (Figures 1 to Figure 4).

Specifically, PIBRENTASVIR possesses a large branched structure, allowing it to interact extensively within the ^{SUB}P pocket and partially within the ^{SAM}P pocket (Figure 1). PIBRENTASVIR exhibited strong interactions with these two pockets, as evidenced by a high ligand-protein contact surface (Figure 1). Interaction analysis between PIBRENTASVIR and MTase revealed that PIBRENTASVIR formed five hydrophobic interactions with residues PHE1667, LEU1720, ASP1725, ALA1780 and LYS1843; four hydrogen bonds with LEU1720, ASP1755, ALA1756 and SER1847 and two halogen bonds with ARG1662 and THR1670 via two fluorine atoms (Figure 1) (Table 1).

The ELBASVIR molecule exhibited a binding orientation along the ^{SUB}P and ^{SAM}P pockets (Figure 2). It demonstrated strong surface contact with MTase in the ^{SAM}P pocket, although its backbone showed relatively weaker interactions (Figure 2). Interaction analysis between ELBASVIR and MTase revealed multiple binding features. Specifically, ELBASVIR formed hydrophobic interactions with residues PRO1656, ASP1725, ALA1780, GLU1781 and ILE1990 (Table 1). Additionally, it established eight hydrogen bonds with residues LEU1654, GLN1658, LEU1720, ASP1725, ASP1755, ALA1756, GLU1781 and LYS1843, along with one π-cation interaction with LYS1991 (Figure 2) (Table 1).

The RITONAVIR molecule was primarily bound within the ^{SAM}P pocket with partial extension into the SUBP pocket (Figure 3). It exhibited strong surface contact with the ^{SAM}P pocket, whereas its interaction area with the SUBP pocket was relatively moderate. Interaction analysis of

RITONAVIR and MTase was conducted using the PLIP server. The results revealed that RITONAVIR formed hydrophobic interactions with residues LEU1720, ALA1756 and GLU1781 (Figure 3) (Table 1). Among the selected molecules, RITONAVIR displayed the highest number of hydrogen bonds with MTase, forming a total of 10 hydrogen bonds with residues ARG1662, LYS1673, LEU1720, GLU1781, LYS1817, LYS1843, GLY1846, GLU1848 and LYS1871 (Figure 3) (Table 1).

We observed that REMDESIVIR was neatly embedded within the ^{SAM}P pocket (Figure 4). Surface interaction analysis between REMDESIVIR and MTase indicated that the drug molecule was deeply positioned within the pocket, exhibiting good surface contact, except for the outer region of the pocket, where the interaction area was relatively limited. An analysis of the MTase residues forming interactions with REMDESIVIR was conducted. The results showed that REMDESIVIR established a total of five hydrophobic interactions with residues ALA1699, LEU1724, ASP1725, GLU1781 and PHE1782 (Figure 4) (Table 1). Additionally, it formed seven hydrogen bonds with residues GLY1696, LEU1720, THR1754, ASP1755, ALA1756 and GLU1781, as well as one salt bridge interaction with residue LYS1817 (Figure 4) (Table 1). REMDESIVIR also exhibited intramolecular interactions, which may contribute to its stable binding within the ^{SAM}P pocket (Figure 4). The interactions formed between MTase and the ligands are summarized in table 1.

Molecular dynamics simulation: Molecular dynamics (MD) simulations of MTase-drug complexes were performed to determine the stability of interactions between the ligands and the protein. Additionally, these simulations assessed structural changes in MTase upon binding to each drug molecule compared to its natural ligand, GTP. We evaluated protein fluctuations over the 100 ns simulation by calculating the root mean square deviation (RMSD) of C_α (Figure 5A).

Table 1
The interaction profile of drugs with MTase.

Compounds	Free energy of binding	Hydrophobic interactions	Hydrogen bonds	π -Cation	Halogen bonds	Salt Bridges
PIBRENTASVIR	-19.2 (kcal/mol)	PHE1667, LEU1720, ASP1725, ALA1780, LYS1843 (Total: 5)	LEU1720, ASP1755, ALA1756, SER1847 (Total: 4)	-	ARG1662, THR1670 (Total: 2)	-
ELBASVIR	-16.42 (kcal/mol)	PRO1656, ASP1725, ALA1780, GLU1781, ILE1990 (Total: 5)	LEU1654, GLN1658, LEU1720, ASP1725, ASP1755, ALA1756, GLU1781, LYS1843 (Total: 8)	LYS1991 (Total: 1)	-	-
RITONAVIR	-15.61 (kcal/mol)	LEU1720, ALA1756, GLU1781 (Total: 4)	ARG1662, LYS1673, LEU1720, GLU1781, LYS1817, LYS1843, GLY1846, GLU1848, LYS1871 (Total: 10)	-	-	-
REMDESIVIR	-13.20 (kcal/mol)	ALA1699, LEU1724, ASP1725, GLU1781, PHE1782 (Total: 5)	GLY1696, LEU1720, THR1754, ASP1755, ALA1756, GLU1781 (Total: 7)	-	-	LYS1871 (Total: 1)

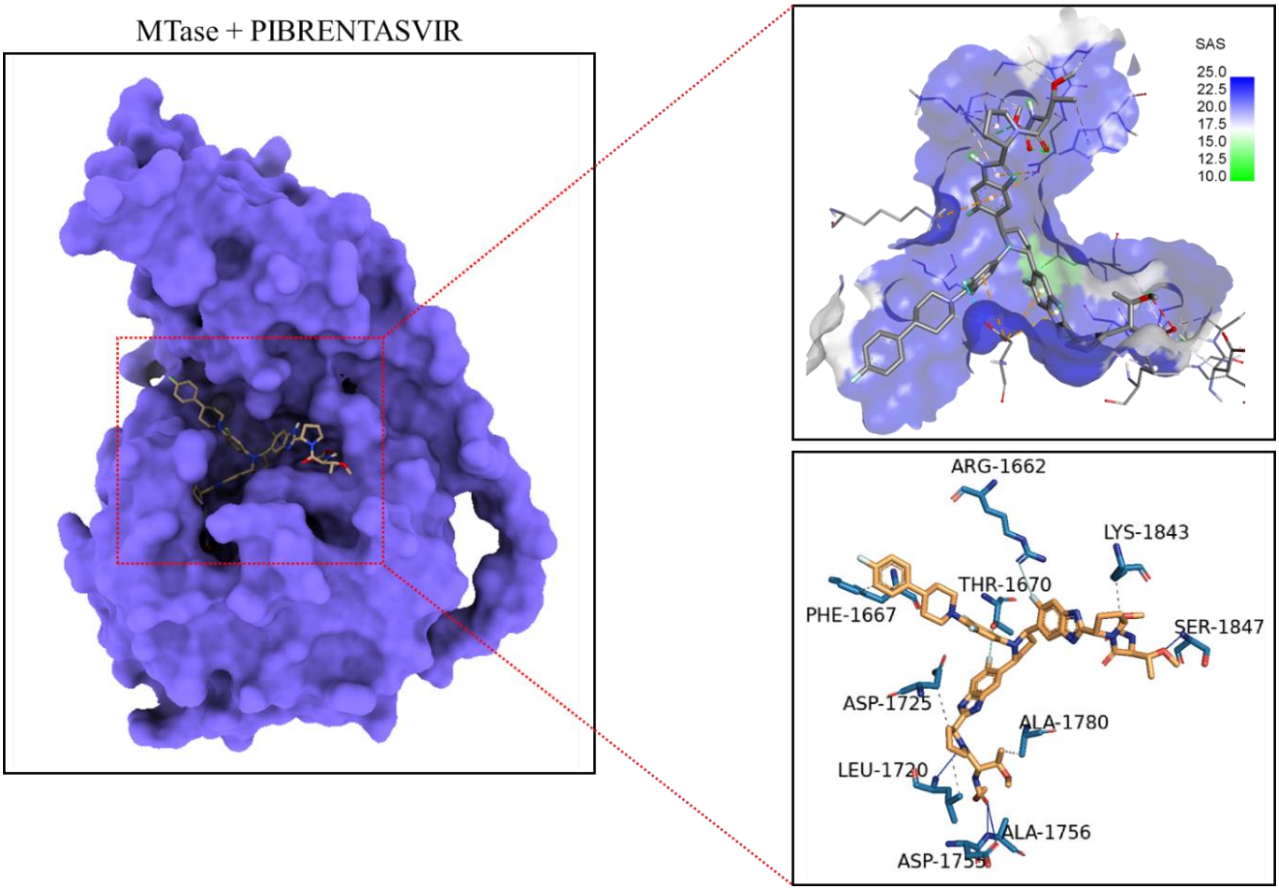

Figure 1: The binding pose of PIBRENTASVIR in MTase of HMPV.

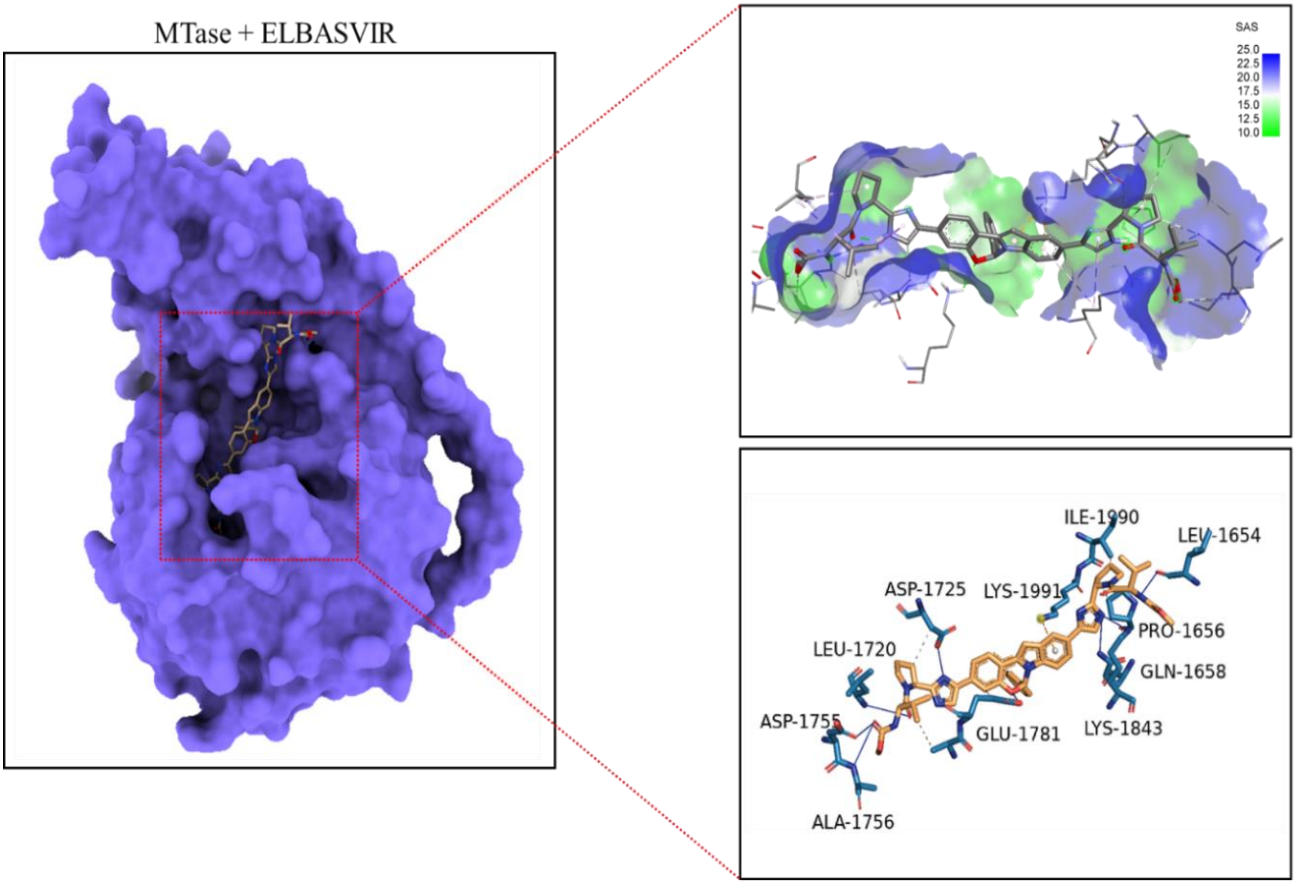

Figure 2: The binding pose of ELBASVIR in MTase of HMPV.

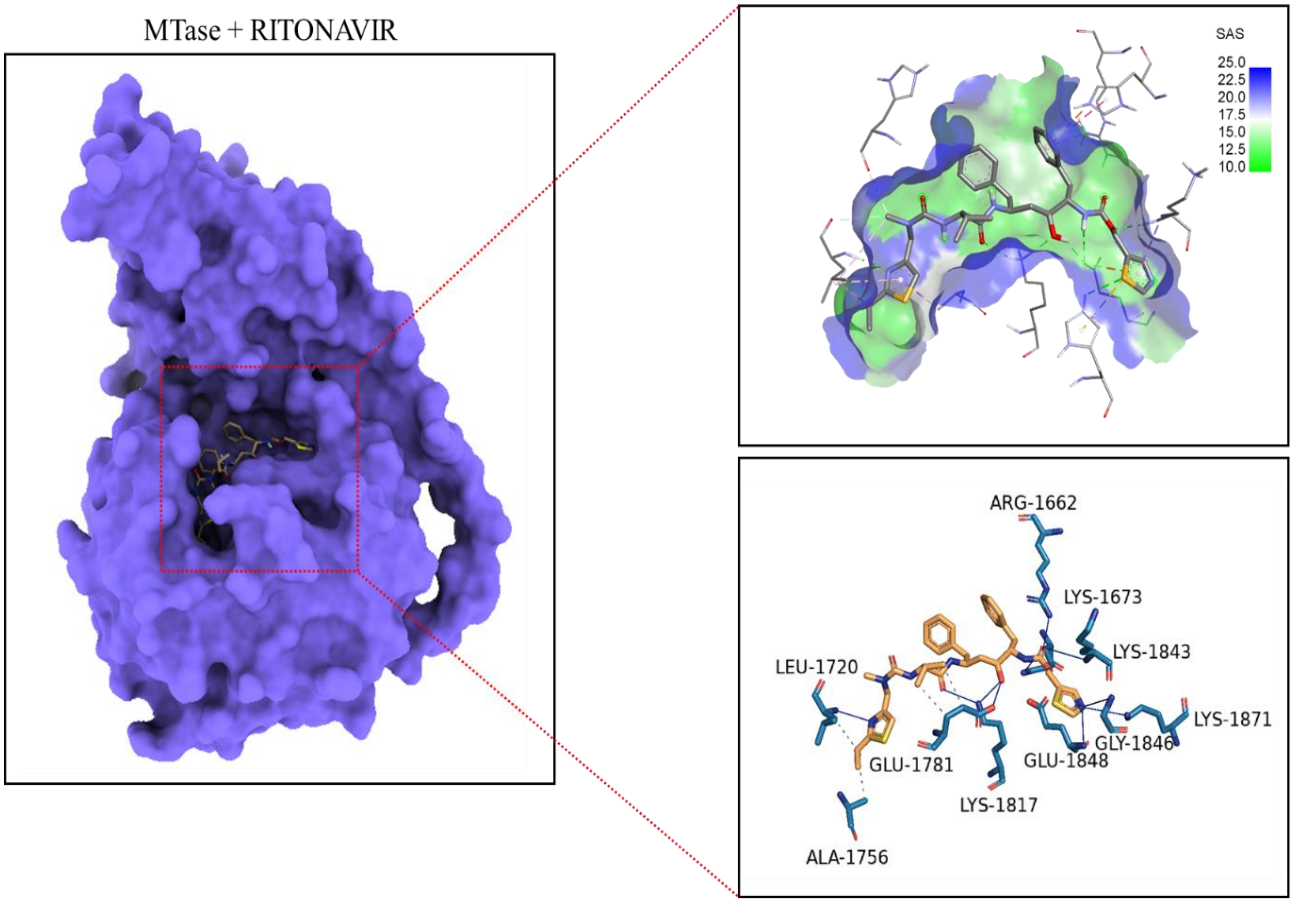

Figure 3: The binding pose of RITONAVIR in MTase of HMPV.

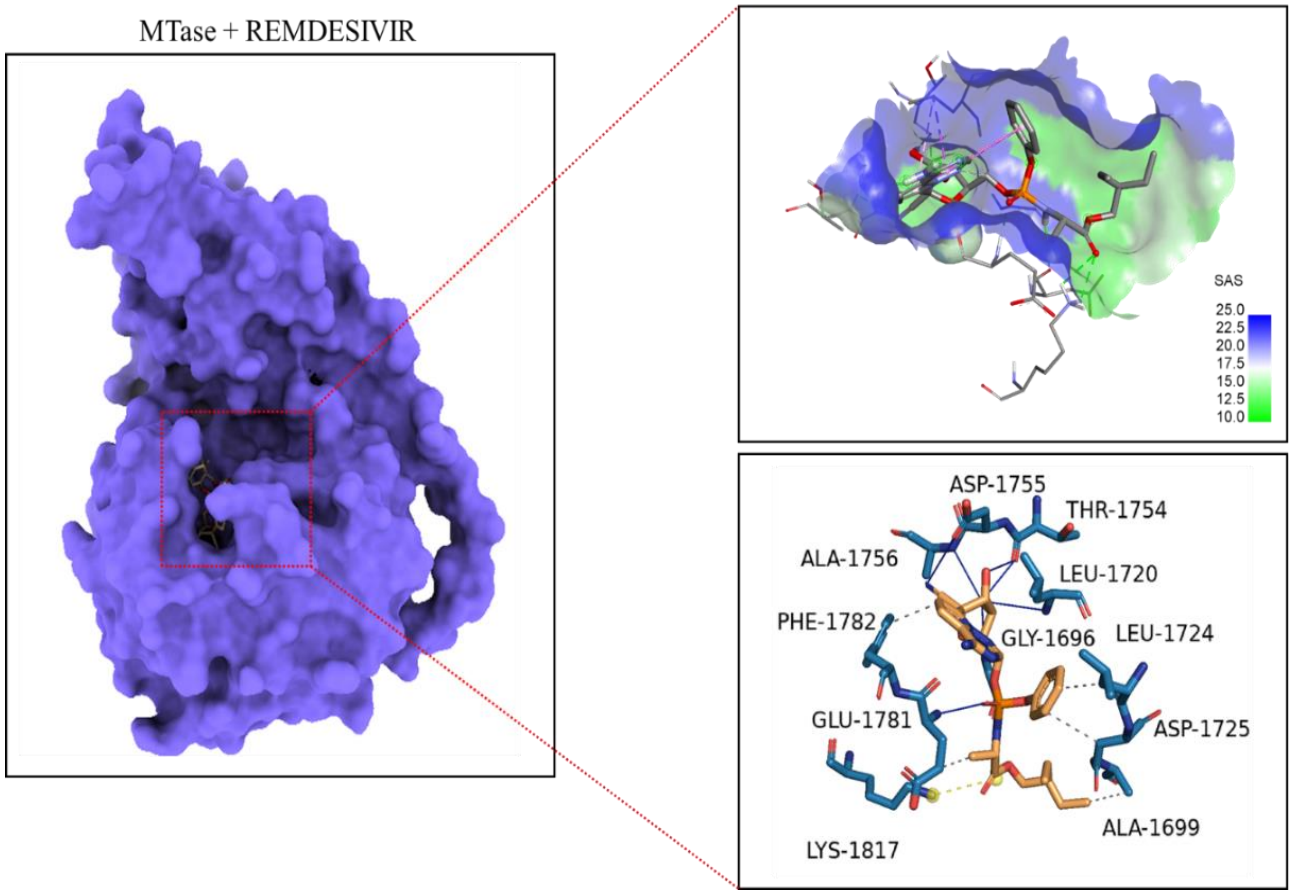

Figure 4: The binding pose of REMDESIVIR in MTase of HMPV.

The RMSD analysis over the 100 ns simulation indicated that MTase exhibited greater structural stability when interacting with the drug molecules compared to GTP (Figure 5A). This observation was further supported by the average RMSD values of each simulated complex corresponding to MTase + GTP, MTase + PIBRENTASVIR, MTase + ELBASVIR, MTase + RITONAVIR and MTase + REMDESIVIR which were 0.323 ± 0.048 nm, 0.245 ± 0.029 nm, 0.245 ± 0.024 nm, 0.295 ± 0.032 nm and 0.234 ± 0.018 nm respectively (Figure 5B).

Radius of gyration (Rg) analysis was performed to evaluate the compactness of MTase over the 100 ns simulation in the presence of different ligands. The time-dependent Rg profiles indicated that MTase underwent changes in its structural compactness when interacting with the newly introduced ligands (Figure 5C). Notably, MTase exhibited a more compact structure in the presence of the drug molecules compared to GTP throughout the 100 ns simulation (Figure 5C). This observation was further supported by the average Rg values for MTase in the complexes MTase + GTP, MTase + PIBRENTASVIR, MTase + ELBASVIR, MTase + RITONAVIR and MTase + REMDESIVIR which were 2.370 ± 0.022 nm, 2.299 ± 0.022 nm, 2.302 ± 0.018 nm, 2.296 ± 0.015 nm and 2.276 ± 0.011 nm respectively (Figure 5D).

Although the drug molecules possess more complex molecular structures than GTP, their interaction with MTase resulted in a more tightly folded protein conformation (Figures 5C and 5D). This suggests that the strong interactions between the drug molecules and the protein induce minor changes in the overall structure of MTase. We also performed a solvent accessible surface area (SASA) analysis of MTase over the 100 ns simulation to evaluate the accessibility of water molecules to the protein.

The SASA values of MTase in the presence of different ligands over the 100 ns simulation are shown in figure 5E. The results indicated that MTase exhibited a higher SASA when interacting with GTP compared to other ligands. This was reflected in the average SASA values of MTase in each simulated system: MTase + GTP, MTase + PIBRENTASVIR, MTase + ELBASVIR, MTase + RITONAVIR and MTase + REMDESIVIR, with respective values of 206.120 ± 3.569 nm/S2/N, 194.544 ± 3.305 nm/S2/N, 194.066 ± 2.452 nm/S2/N, 188.332 ± 3.342 nm/S2/N and 191.589 ± 2.977 nm/S2/N. These findings suggest that PIBRENTASVIR, ELBASVIR, RITONAVIR and REMDESIVIR occupy the binding pockets, thereby restricting solvent access to these regions. This indicates that the drug molecules remain stably positioned within the predicted binding pockets, potentially inhibiting MTase activity.

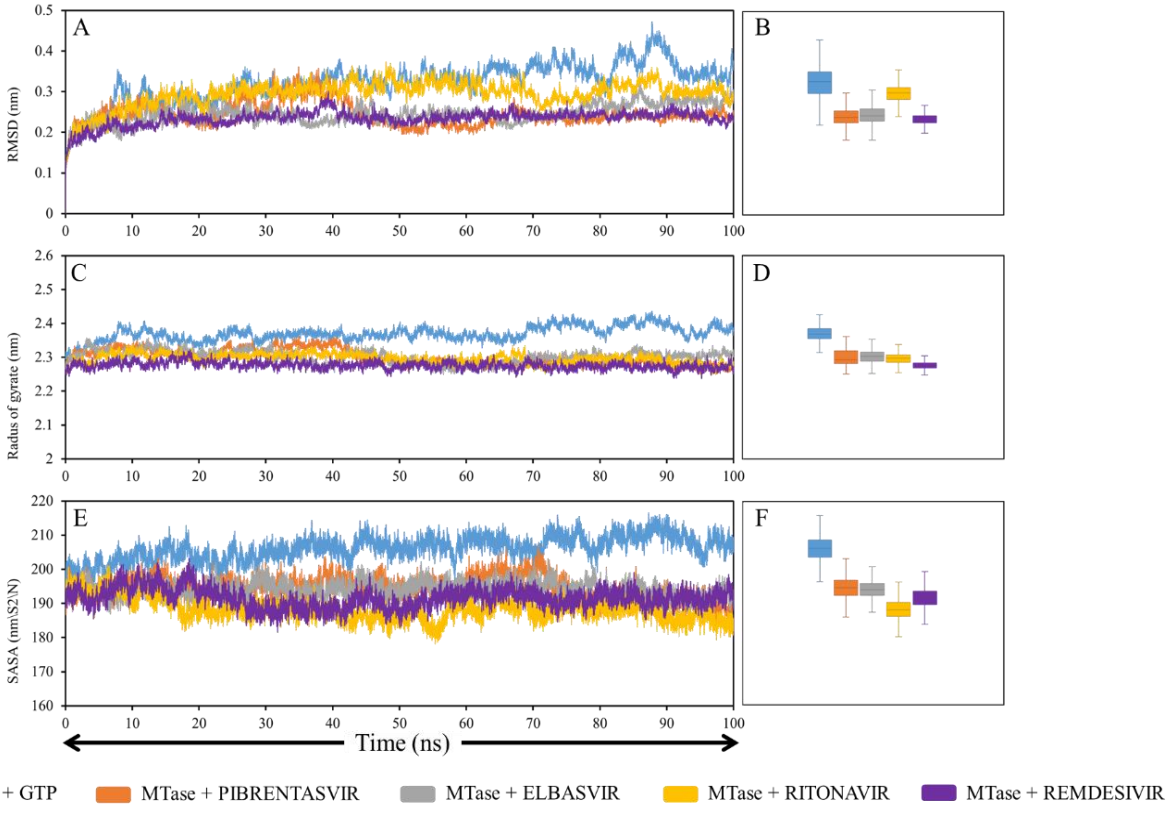

Figure 5: Root mean square-deviation (RMSD), radius of gyrate (Rg) and solvent accessible surface area (SASA) of MTase in complex with each ligand.
A. RMSD value per time. B. Average of RMSD. C. Rg value per time. D. Average of Rg. E. SASA value per time. F. Average of SASA. The colors shown for each particular system: blue: MTase + GTP; organge: MTase + PIBRENTASVIR; gray: MTase + ELBASVIR; yellow: MTase + RITONAVIR; purple: MTase + REMDESIVIR.

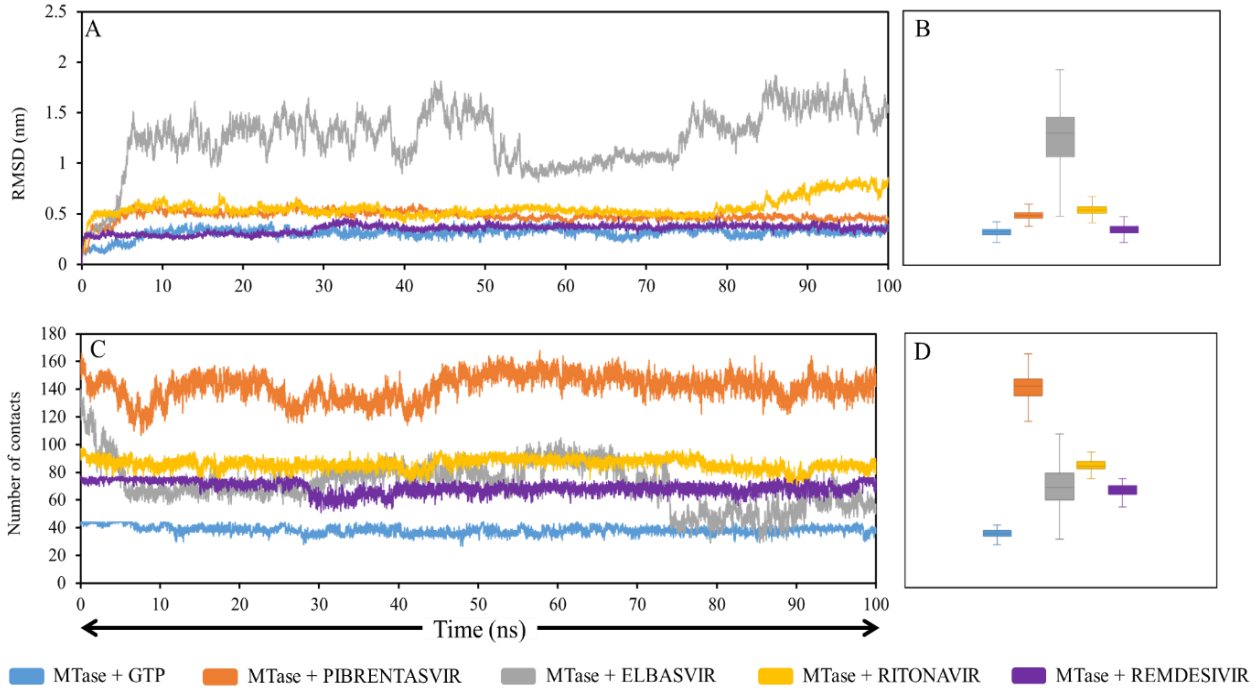

Figure 6: RMSD of ligand fit on MTase and number of contacts between ligand and MTase in MD simulations. A. RMSD of ligand fit on protein per time. B. Average of RMSD. C. Number of contacts value per time. D. Average of number of contacts. The colors shown for each particular system: blue: MTase + GTP; organge: MTase + PIBRENTASVIR; gray: MTase + ELBASVIR; yellow: MTase + RITONAVIR; purple: MTase + REMDESIVIR.

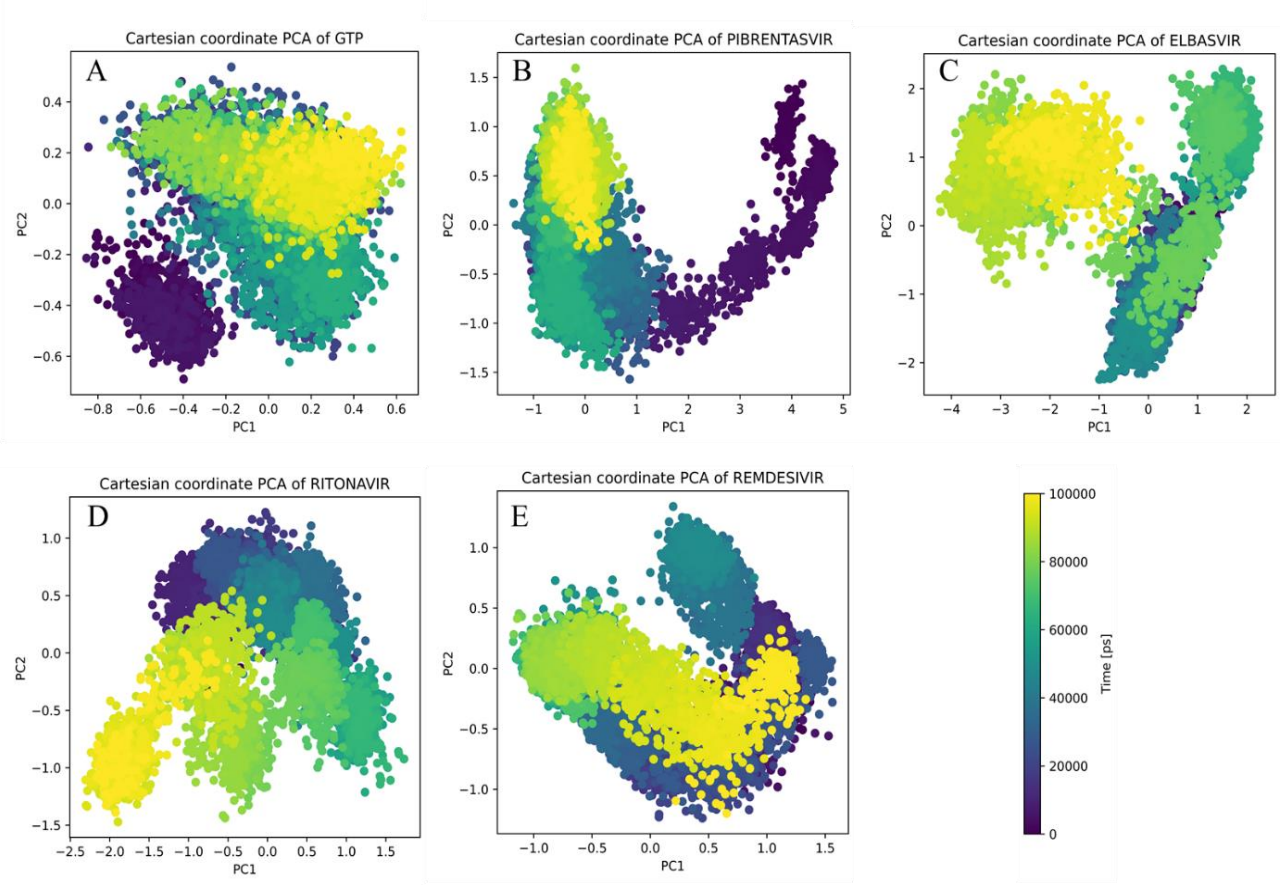

Figure 7: Principal component analysis (PCA) of each ligand in 100 ns simulation. Each dot represents the structural state of the ligand captured at a given time frame. The color scale indicates the sampling time. A total of 10,000 samples were collected over the 100 ns simulation.

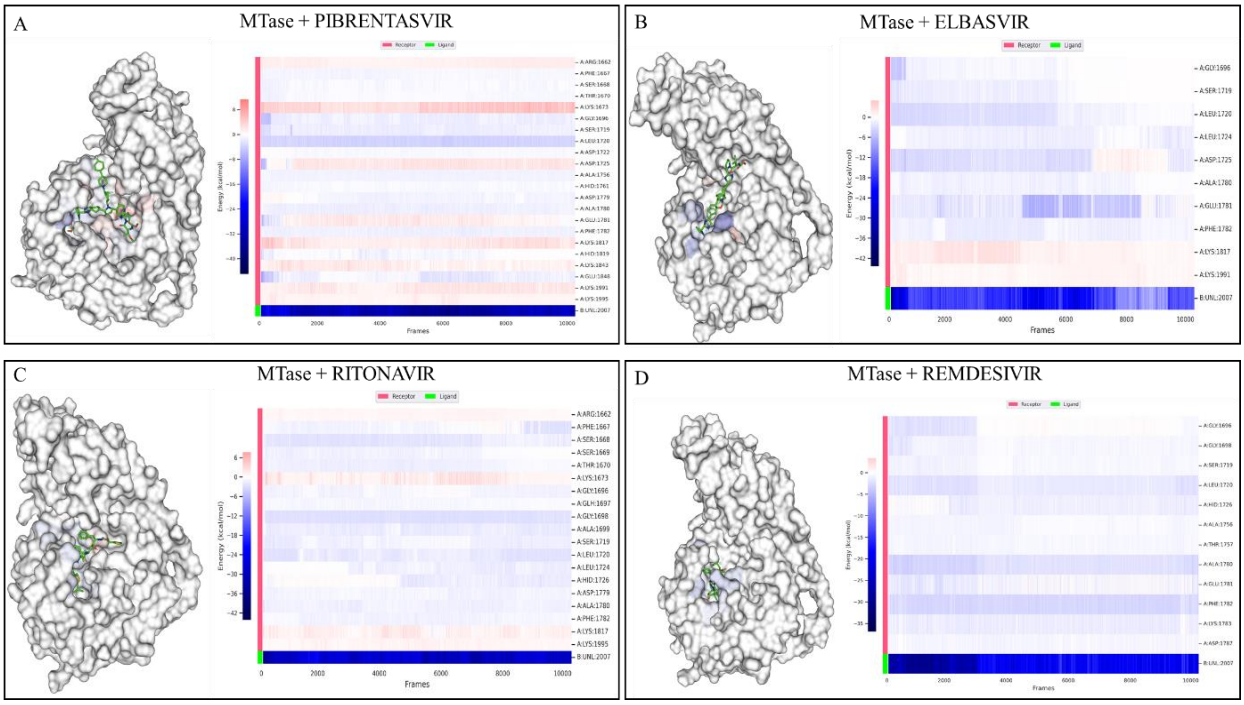

Figure 8: De-composite analysis of amino acid interaction energy of MTase with each ligand in 100 ns simulation

Next, we assessed the stability of the ligands during their interaction with MTase over the 100 ns simulation by analyzing the RMSD of the ligand fit on the protein. The results revealed that ELBASVIR exhibited a high RMSD value of 1.251 ± 0.297 nm, indicating significant fluctuations and lower stability of the ligand (Figures 6A and 6B). This instability is likely due to its weaker interaction with MTase in the ^{SUB}P pocket, leading to its repositioning within the binding site during the simulation (Figure 2). In contrast, the other ligands including GTP, PIBRENTASVIR, RITONAVIR and REMDESIVIR, demonstrated greater stability throughout the 100 ns simulation, with recorded average RMSD values of 0.314 ± 0.052 nm, 0.481 ± 0.054 nm, 0.558 ± 0.091 nm and 0.349 ± 0.042 nm respectively (Figures 6A and 6B). Furthermore, the stable interaction of the ligands with MTase was also reflected in the total number of contacts each ligand maintained with the protein.

We analyzed the number of contacts of each ligand with MTase over the 100 ns simulation. The results showed that all ligands remained in contact with MTase throughout the simulation (Figure 6C). As previously mentioned, ELBASVIR exhibited significant fluctuations, leading to less stable contacts with the protein and a tendency to decrease toward the end of the simulation, with an average of 71 ± 16 contacts recorded (Figure 6D).

In contrast, the other drug molecules PIBRENTASVIR, RITONAVIR and REMDESIVIR, demonstrated higher numbers of contacts with MTase compared to GTP, with average values of 142 ± 9 contacts, 86 ± 4 contacts, 69 ± 4 contacts and 38 ± 3 contacts respectively (Figures 6C and 6D). These findings indicate that PIBRENTASVIR, RITONAVIR and REMDESIVIR can establish stable interactions within the MTase pocket during the 100 ns simulation.

Principal component analysis (PCA) was performed to determine structural variations of the ligands during the simulation. This analysis captures different structural states of the ligands at each time point and their convergence behavior. The molecular structure of GTP over 100 ns was found to be oriented along the positive axis in both PC1 and PC2, gradually converging towards zero, indicating a stable and balanced structural state (Figure 7A). PIBRENTASVIR initially exhibited minor structural fluctuations but subsequently achieved convergence in both PC1 and PC2 (Figure 7B), suggesting that its molecular structure converged (Figure 7B). In contrast, ELBASVIR displayed structural variations in its interaction with MTase, as revealed by PCA analysis (Figure 7C). The collected structures of ELBASVIR did not follow a specific trend along PC1 or PC2 but instead formed two distinct clusters (Figure 7C), indicating a lack of structural convergence and significant fluctuations during the simulation.

A similar behavior was observed for RITONAVIR, which also exhibited multiple structural clusters in the PCA analysis (Figure 7D). On the other hand, REMDESIVIR showed a high degree of structural convergence and reached equilibrium, as indicated by the near-overlapping sampled structures (Figure 7E). Overall, the PCA analysis demonstrated structural variations of the ligands over the 100 ns simulation when interacting with MTase. The results suggest that PIBRENTASVIR and REMDESIVIR remained relatively stable with minimal structural changes during the simulation whereas ELBASVIR and RITONAVIR underwent molecular structural alterations.

Table 2
The average of BFE value of drug in complex with MTase (kcal/mol).

	GTP	PIBRENTASVIR	ELBASVIR	RITONAVIR	REMDESIVIR
ΔG_{vdW}	-22.31 ± 3.78	-80.77 ± 5.28	-32.47 ± 9.52	-64.68 ± 4.64	-48.52 ± 7.89
ΔG_{Ele}	-1151.36 ± 67.93	819.95 ± 64.89	541.48 ± 67.92	-25.53 ± 9.31	-53.24 ± 12.00
ΔG_{Pol}	1166.42 ± 58.88	-764.21 ± 62.75	-528.46 ± 64.82	56.52 ± 8.13	73.11 ± 10.88
ΔG_{npol}	-4.21 ± 0.54	-10.20 ± 0.63	-4.59 ± 1.31	-7.78 ± 0.64	-6.20 ± 0.87
$\Delta G_{MM/GBSA}$	-11.47 ± 14.62	-35.23 ± 6.44	-24.04 ± 10.26	-41.48 ± 5.43	-34.85 ± 8.87

Binding free energy and decomposite analysis: Binding free energy (BFE) is a crucial parameter for determining the affinity of a ligand for its target protein. We employed the MM/GBSA model to estimate BFE. The results indicate that GTP, PIBRENTASVIR and REMDESIVIR exhibit stable BFE values whereas ELBASVIR and RITONAVIR display significant fluctuations. The average BFE values for each ligand over 100 ns were calculated and are summarized in table 2. The findings reveal that the drug molecules PIBRENTASVIR, ELBASVIR, RITONAVIR and REMDESIVIR exhibit higher BFE values compared to GTP when binding to MTase with respective values of -35.23 ± 6.44 kcal/mol, -24.04 ± 10.26 kcal/mol, -41.48 ± 5.43 kcal/mol, -34.85 ± 8.87 kcal/mol and -11.47 ± 14.62 kcal/mol.

Additionally, we analyzed the residues involved in ligand interactions and found that the drug molecules maintained stable binding energy with key residues LYS1673, ASP1779, LYS1817 and GLU1848. These residues play a crucial role in the O-2' and N7 methylation processes of MTase (Figure 8). Consequently, our results suggest that these drug molecules have strong binding potential to MTase and can competitively target the active site against GTP (Table 2). This implies their potential to inhibit the protein's enzymatic function, making them promising candidates for HMPV treatment. Moreover, the retention of these molecules within the ^{SAM}P pocket further supports their potential as broad-spectrum inhibitors, as this pocket is conserved in *Pneumovirinae*.

The emergence or re-emergence of viral outbreaks has highlighted the urgent need for effective therapeutic or preventive strategies. Drug repositioning is a strategy that identifies new therapeutic applications for approved or investigational drugs beyond their original indications, facilitating the development of antiviral treatments[22]. The conventional antiviral drug development process is time-consuming and resource-intensive, often spanning decades and costing billions of dollars. Since the repurposed drugs already have established clinical evidence and safety profiles, the next objective is to further validate their efficacy in the target population and progress through phase III clinical trials. To accelerate drug screening and optimize therapeutic targets, high-throughput *in silico* screening has been widely adopted[11,30,32].

In silico screening is commonly used to identify compounds that bind to specific viral protein targets such as RdRp which is often conserved among various viral groups, particularly RNA viruses[23]. In the present study, we conducted a detailed molecular interaction analysis of antiviral compounds from the e-Drug3D library. Our findings identified PIBRENTASVIR, ELBASVIR, RITONAVIR and the broad-spectrum antiviral REMDESIVIR as potential inhibitors of HMPV MTase activity. These drugs have been approved by the FDA for the treatment of specific viral infections.

Notably, REMDESIVIR has been shown to inhibit the RdRp activity of multiple viruses by competing with ATP, leading to premature termination of RNA synthesis in Ebola virus and MERS-CoV after approximately 3 to 5 nucleotides[8,27,35]. Although PIBRENTASVIR and ELBASVIR have not yet been classified as broad-spectrum antivirals, they share a similar mechanism of action by inhibiting an RNA-binding protein[9,13]. In contrast, RITONAVIR functions through a different mechanism, targeting HIV-1 protease. However, it has also been investigated for the treatment of SARS-CoV and MERS-CoV when combined with LOPINAVIR[4,10]. During the COVID-19 pandemic, the RITONAVIR-LOPINAVIR combination was used as a treatment for SARS-CoV-2-infected patients[16].

In this study, we demonstrated that these drug molecules can bind to the ^{SAM}P or ^{SUB}P pocket of HMPV MTase. These initial findings lay the groundwork for future *in vitro* and *in vivo* studies to confirm their inhibitory effects on HMPV. Furthermore, our results support the discovery of novel broad-spectrum antiviral drugs or preventive strategies against respiratory viral infections. While *in silico* computational methods attempt to model the biological characteristics and functions of HMPV MTase as accurately as possible, they still have limitations in docking and MD simulations. Therefore, future research should focus on *in vitro* and *in vivo* analyses to validate the HMPV inhibitory potential of these drug candidates.

Conclusion

Our study leverages an FDA-approved drug library to screen for potential antiviral compounds for HMPV treatment. We have identified PIBRENTASVIR, ELBASVIR, RITONAVIR and REMDESIVIR as promising drug candidates for HMPV treatment, as they exhibit the ability to bind to the viral MTase. *In silico* analysis revealed that these compounds bind to the active site of MTase and maintain stable chemical interactions throughout a 100 ns simulation. Moreover, they demonstrate higher binding

affinity than GTP, suggesting their potential to competitively inhibit MTase activity.

Acknowledgement
This work is a part of the research project CS.2025.A4.015 funded by Saigon University.

References
1. Abraham M.J., Murtola T., Schulz R., Páll S., Smith J.C., Hess B. and Lindahl E.J.S., GROMACS: High performance molecular simulations through multi-level parallelism from laptops to supercomputers, *SoftwareX*, **1**, 19-25 **(2015)**

2. Adasme M.F., Linnemann K.L., Bolz S.N., Kaiser F., Salentin S., Haupt V.J. and Schroeder M., PLIP 2021: expanding the scope of the protein–ligand interaction profiler to DNA and RNA, *Nucleic. Acids. Res.*, **49**(**W1)**, W530-W534 **(2021)**

3. Amarasinghe G.K. et al, Taxonomy of the order Mononegavirales: update 2018, *Arch. Virol*., **163(8)**, 2283-2294 **(2018)**

4. Chu C.M. et al, Role of lopinavir/ritonavir in the treatment of SARS: initial virological and clinical findings, *Thorax*, **59**(**3)**, 252-256 **(2004)**

5. Costa-Filho R.C., Saddy F., Costa J.L.F., Tavares L.R. and Castro Faria Neto H.C., The Silent Threat of Human Metapneumovirus: Clinical Challenges and Diagnostic Insights from a Severe Pneumonia Case, *Microorganisms*, **13**(**1)**, 73 **(2025)**

6. Divarathna M.V.M., Rafeek R.A.M. and Noordeen F., A review on epidemiology and impact of human metapneumovirus infections in children using TIAB search strategy on PubMed and PubMed Central articles, *Rev. Med. Virol*., **30(1)**, e2090 **(2020)**

7. Du Y. et al, Epidemiology and genetic characterization of human metapneumovirus in pediatric patients from Hangzhou China, *J. Med. Virol*., **94(11)**, 5401-5408 **(2022)**

8. Gordon C.J., Tchesnokov E.P., Feng J.Y., Porter D.P. and Götte M., The antiviral compound remdesivir potently inhibits RNA-dependent RNA polymerase from Middle East respiratory syndrome coronavirus, *J. Biol. Chem.*, **295(15)**, 4773-4779 **(2020)**

9. Huang L., Hwang J., Sharma S.D., Hargittai M.R., Chen Y., Arnold J.J., Raney K.D. and Cameron C.E., Hepatitis C virus nonstructural protein 5A (NS5A) is an RNA-binding protein, *J. Biol. Chem*., **280(43)**, 36417-36428 **(2005)**

10. Hushmandi K., Bokaie S., Hashemi M., Moghadam E.R., Raei M., Hashemi F., Bagheri M., Habtemariam S. and Nabavi S.M., A review of medications used to control and improve the signs and symptoms of COVID-19 patients, *Eur. J. Pharmacol*., **887**, 173568 **(2020)**

11. Janes J. et al, The ReFRAME library as a comprehensive drug repurposing library and its application to the treatment of cryptosporidiosis, Proc. Natl. Acad. Sci. U.S.A., **115(42)**, 10750-10755 **(2018)**

12. Jefferson T. et al, Physical interventions to interrupt or reduce the spread of respiratory viruses, *Cochrane Database Syst. Rev*., **1(1)**, Cd006207 **(2023)**

13. Keating G.M., Elbasvir/Grazoprevir: First Global Approval, *Drugs*, **76**(**5)**, 617-624 **(2016)**

14. Lee J. et al, CHARMM-GUI Input Generator for NAMD, GROMACS, AMBER, OpenMM and CHARMM/OpenMM Simulations Using the CHARMM36 Additive Force Field, *J. Chem. Theory Comput*., **12(1)**, 405-413 **(2016)**

15. Li X. and Peng T., Strategy, Progress and Challenges of Drug Repurposing for Efficient Antiviral Discovery, *Front. Pharmacol*., **12**, 660710 **(2021)**

16. Lim J. et al, Case of the Index Patient Who Caused Tertiary Transmission of COVID-19 Infection in Korea: the Application of Lopinavir/Ritonavir for the Treatment of COVID-19 Infected Pneumonia Monitored by Quantitative RT-PCR, *J. Korean Med. Sci*., **35(6)**, e79 **(2020)**

17. Ma S. et al, Development of a novel multi-epitope mRNA vaccine candidate to combat HMPV virus, *Hum. Vaccin. Immunother*., **19(3)**, 2293300 **(2023)**

18. McGibbon R.T. et al, MDTraj: A Modern Open Library for the Analysis of Molecular Dynamics Trajectories, *Biophys. J*., **109(8)**, 1528-1532 **(2015)**

19. Morris G.M., Huey R., Lindstrom W., Sanner M.F., Belew R.K., Goodsell D.S. and Olson A.J., AutoDock4 and AutoDockTools4: Automated docking with selective receptor flexibility, *J. Comput. Chem*., **30(16)**, 2785-2791 **(2009)**

20. O'Boyle N.M., Banck M., James C.A., Morley C., Vandermeersch T. and Hutchison G.R., Open Babel: An open chemical toolbox, *J. Cheminform*., **3(1)**, 33 **(2011)**

21. Paesen G.C., Collet A., Sallamand C., Debart F., Vasseur J.J., Canard B., Decroly E. and Grimes J.M., X-ray structure and activities of an essential Mononegavirales L-protein domain, *Nat. Commun.*, **6(1)**, 8749 **(2015)**

22. Palacios-Rápalo S.N., Cordero-Rivera C.D., De Jesús-González L.A., Farfan-Morales C.N., Benitez-Vega M., Reyes-Ruiz J.M. and Del Angel R.M., Drug Repositioning as an Antiviral Strategy Against Emerging Viruses, Springer Nature Switzerland, Cham, 273-317 **(2024)**

23. Patel H. and Kukol A., Evolutionary conservation of influenza A PB2 sequences reveals potential target sites for small molecule inhibitors, *Virology*, **509**, 112-120 **(2017)**

24. Pihan E., Colliandre L., Guichou J.F. and Douguet D., e-Drug3D: 3D structure collections dedicated to drug repurposing and fragment-based drug design, *Bioinformatics*, **28(11)**, 1540-1541 **(2012)**

25. Rahmeh A.A., Schenk A.D., Danek E.I., Kranzusch P.J., Liang B., Walz T. and Whelan S.P.J., Molecular architecture of the vesicular stomatitis virus RNA polymerase, Proc. Natl. Acad. Sci. U.S.A., **107(46)**, 20075-20080 **(2010)**

26. Santos-Martins D., Solis-Vasquez L., Tillack A.F., Sanner M.F., Koch A. and Forli S., Accelerating AutoDock4 with GPUs and Gradient-Based Local Search, *J. Chem. Theory Comput.*, **17(2)**, 1060-1073 **(2021)**

27. Tchesnokov E.P., Feng J.Y., Porter D.P. and Götte M., Mechanism of Inhibition of Ebola Virus RNA-Dependent RNA Polymerase by Remdesivir, *Viruses*, **11(4)**, 326 **(2019)**

28. Thammawat S., Sadlon T.A., Hallsworth P.G. and Gordon D.L., Role of cellular glycosaminoglycans and charged regions of viral G protein in human metapneumovirus infection, *J. Virol*., **82(23)**, 11767-11774 **(2008)**

29. Tian C. et al, ff19SB: Amino-Acid-Specific Protein Backbone Parameters Trained against Quantum Mechanics Energy Surfaces in Solution, *J. Chem. Theory Comput*., **16(1)**, 528-552 **(2020)**

30. Ulferts R. et al, Screening of a Library of FDA-Approved Drugs Identifies Several Enterovirus Replication Inhibitors That Target Viral Protein 2C, *Antimicrob. Agents. Chemother.*, **60(5)**, 2627-2638 **(2016)**

31. Valdés-Tresanco M.S., Valdés-Tresanco M.E., Valiente P.A. and Moreno E., gmx_MMPBSA: A New Tool to Perform End-State Free Energy Calculations with GROMACS, *J. Chem. Theory Comput*., **17(10)**, 6281-6291 **(2021)**

32. van Cleef K.W., Overheul G.J., Thomassen M.C., Kaptein S.J., Davidson A.D., Jacobs M., Neyts J., van Kuppeveld F.J. and van Rij R.P., Identification of a new dengue virus inhibitor that targets the viral NS4B protein and restricts genomic RNA replication, *Antiviral Res*., **99(2)**, 165-171 **(2013)**

33. van den Hoogen B.G., Bestebroer T.M., Osterhaus A.D. and Fouchier R.A., Analysis of the genomic sequence of a human metapneumovirus, *Virology*, **295(1)**, 119-132 **(2002)**

34. van den Hoogen B.G., de Jong J.C., Groen J., Kuiken T., de Groot R., Fouchier R.A. and Osterhaus A.D., A newly discovered human pneumovirus isolated from young children with respiratory tract disease, *Nat. Med*., **7(6)**, 719-724 **(2001)**

35. Warren T.K. et al, Therapeutic efficacy of the small molecule GS-5734 against Ebola virus in rhesus monkeys, *Nature*, **531(7594)**, 381-385 **(2016)**

36. Ye W. et al, Remdesivir (GS-5734) Impedes Enterovirus Replication Through Viral RNA Synthesis Inhibition, *Front. Microbiol*., **11**, 1105 **(2020)**.

(Received 20th August 2025, accepted 19th September 2025)